CNS Neuroscience & Therapeutics

ORIGINAL ARTICLE

CNS Neuroscience & Therapeutics

Neonatal Maternal Deprivation Enhances Presynaptic P2X7 Receptor Transmission in Insular Cortex in an Adult Rat Model of Visceral Hypersensitivity

Ping-An Zhang,[1] Qi-Ya Xu,[1] Lu Xue,[1] Hang Zheng,[1] Jun Yan,[2] Ying Xiao[1,3] & Guang-Yin Xu[1]

1 Jiangsu Key Laboratory of Translational Research and Therapy for Neuro-Psycho-Diseases, Laboratory of Translational Pain Medicine, Institute of Neuroscience, Soochow University, Suzhou, China
2 The Second Affiliated Hospital of Soochow University, Suzhou, China
3 Chengdu Radio and TV University, Chengdu, China

Keywords
Insular cortex; Neonatal maternal deprivation; Purinergic P2X receptors; Visceral pain.

Correspondence
G.-Yin Xu, M.D., Ph.D., and Y. Xiao, Ph.D., Laboratory of Translational Pain Medicine, Institute of Neuroscience, Soochow University, Suzhou 215123, China.
Tel.: +86-512-65882817 and +86-512-65882539;
Fax: +86-512-65883602 and +86-512-65883602;
E-mails: guangyinxu@suda.edu.cn and et790906@hotmail.com
Received 27 August 2016; revision 6 October 2016; accepted 11 November 2016

SUMMARY

Aims: Insular cortex (IC) is involved in processing the information of pain. The aim of this study was to investigate roles and mechanisms of P2X7 receptors (P2X7Rs) in IC in development of visceral hypersensitivity of adult rats with neonatal maternal deprivation (NMD). **Methods:** Visceral hypersensitivity was quantified by abdominal withdrawal reflex threshold to colorectal distension (CRD). Expression of P2X7Rs was determined by qPCR and Western blot. Synaptic transmission in IC was recorded by patch-clamp recording. **Results:** The expression of P2X7Rs and glutamatergic neurotransmission in IC was significantly increased in NMD rats when compared with age-matched controls. Application of BzATP (P2X7R agonist) enhanced the frequency of spontaneous excitatory postsynaptic currents (sEPSC) and miniature excitatory postsynaptic currents (mEPSC) in IC slices of control rats. Application of BBG (P2X7R antagonist) suppressed the frequencies of sEPSC and mEPSC in IC slices of NMD rats. Microinjection of BzATP into right IC significantly decreased CRD threshold in control rats while microinjection of BBG or A438079 into right IC greatly increased CRD threshold in NMD rats. **Conclusion:** Data suggested that the enhanced activities of P2X7Rs in IC, likely through a presynaptic mechanism, contributed to visceral hypersensitivity of adult rats with NMD.

doi: 10.1111/cns.12663

The first two authors contributed equally to this work.

Introduction

The insular cortex (IC), an important component of the limbic system, is involved in processing the sense of taste, emotion, and perception of innocuous warm and cold [1–3]. Recent studies have shown that painful stimuli activate IC and that direct stimulation of IC evokes painful sensations [4,5]. There is a correlation between IC and phantom limb pain [6]. IC plays roles in modulation of both affective and sensory components of pain [7–9]. Although hypersensitivity in patients with irritable bowel syndrome (IBS) is accompanied by increased activities in IC and ACC [10], whether IC is involved in chronic visceral hypersensitivity (CVH) of adult rats with neonatal maternal deprivation (NMD) is unknown.

ATP as an energetic substance for cellular metabolism can be released into extracellular space and plays an important role in mediating fast excitatory neurotransmission [11] as well as calcium waves between astrocytic glial cells [12]. ATP has also been considered to be a neuromodulator [13,14]. The P2X receptors for ATP are ligand-gated nonspecific cation channels [11]. Activation of P2X receptors could directly or indirectly increase synaptic transmission [11]. Among the subtypes of P2X receptors, P2X7 receptors (P2X7Rs) are widely found in central nervous system (CNS) such as cerebral cortex [15–17]. It is usually activated by a high concentration of ATP (>100 μM) *in vivo* [18].

The activation of P2X7Rs is involved in the regulation of calcium-dependent and calcium-independent release of glutamate [19]. Compared with other P2X receptors, P2X7Rs were more commonly seen in the presynaptic sites of CNS including the spinal cord, medulla oblongata and nodose ganglia [20], and excitatory presynaptic terminals in forebrain regions [21]. However, the expression and distribution of P2X7Rs in IC are not clear. Neither is the physiological function of P2X7Rs in the IC in the development of CVH.

In this study, we assumed that P2X7Rs in IC were involved in regulation of visceral hypersensitivity of NMD rats. Integrative approaches, including whole cell patch clamping, Western blotting, qPCR, immunohistochemistry, and behavioral techniques, were used to prove the hypothesis.

Materials and Methods

NMD and Measurement of Chronic Visceral Hyperalgesia (CVH)

Handling of the animals was approved by the Institutional Animal Care and Use Committee at Soochow University and was strictly in accordance with the guidelines of the International Association for the Study of Pain. Pups of male Sprague Dawley rats for NMD group were separated from the maternity cages and placed in isolated cages with an electric blanket to keep them warm (32°C) for 3 h daily from postnatal days 2–15. After the separation period, pups were returned to their maternity cages. Pups for control group (CON) were not exposed to handling. CVH induction and assessment were performed according to the protocol described previously [22,23]. Experiments were performed in these rats at the age of 6–7 weeks.

Drug Administration

For behavioral experiments, BzATP (P2X7R agonist), brilliant blue G (BBG) (P2X7R antagonist), and A438079 (P2X7R antagonist) were diluted by normal saline (NS) (NaCl, wt/v 0.9%). The drugs, NS, or vehicle for A438079 (NS with DMSO) were stereotactically injected into the unilateral IC of rats. It is reported that there is a stronger functional link between right insula and autonomic regions, whereas left anterior regions do not show connectivity with the thalamus at all; there is a more prominent sympathetic role of the right insula [24]. Because NMD mimics the effects of early life stress on the development of emotional and social behaviors, we mainly explored the role of the right IC in the development of visceral hypersensitivity of NMD rats by microinjecting drugs into right IC. A stainless guide cannula with 24 gauge was fixed unilaterally on the right hemisphere of the skull aiming at IC (coordinates with respect to Bregma: AP 0.5 mm, ML 5.6 mm, DV 7.0 mm, angle 0) using dental cement. The drugs, NS, or vehicle (1 μL) were injected into right IC by a needle head through the guide cannula and reached a final depth of 7.5 mm below dura. The way of microinjection was done as described previously [23]. CRD threshold was assessed before drug microinjection and tested once every 5 min after microinjection until the effect of drug totally disappeared. The drug concentrations used in the study were based on our preliminary data and reports from other groups [19,20,25,26].

Western Blotting

The Western blotting process was done as described in our previous reports [23]. The membrane carried P2X7Rs (~90 KD) was incubated with anti-P2X7Rs antibody (1:500, APR004, Alomone Labs, Jerusalem, Israel), and the membrane carried GAPDH (~37KD) was incubated with anti-GAPDH antibody (1:200, sc-25778, Santa Cruz, Dallas, TX, USA). Band intensities were measured using ImageJ software. P2X7Rs protein expression was normalized to GAPDH.

Real-Time qPCR for P2X7R mRNA

Total RNA was extracted from IC of both hemispheres from control and NMD rats with TRIzol (15596026, Ambion, Shanghai, China). cDNA was synthesized from total RNA using an Reverse transcription kit (AE301-03, Transgen Biotech, Beijing, China) following the supplier's instructions. The sequences of the primer pairs for *p2x7r* used in quantitative polymerase chain reaction are as follows: (F) 5′-CGGCACCATCAAGTGGATCTT-3′ and (R) 5′-CT GCAACGCCTTTGACCTTG-3′; the sequence of the primer pairs for *gapdh* (as an internal control) used in quantitative polymerase chain reaction is as follows: (F) 5′ -TGGAGTCTACTGGCGTCTT-3′ and (R) 5′-TGTCATATTTCTCGTGGTTCA-3′. Control reactions were performed without cDNA templates.

Slice Preparation and Whole Cell Patch-Clamp Recordings in the IC

Rats of both control and NMD group (100–130 g, 6–7 weeks of age) were anesthetized with 4% chloral hydrate. Transverse brain slices of the IC (400 μm) were cut using standard methods [23,27] with oxygenated (95% O_2, 5% CO_2) solution (in mM): 93 NMDG, 2.5 KCl, 1.2 NaH_2PO_4, 30 $NaHCO_3$, 20 HEPES, 5 sodium ascorbate, 2 thiourea, 3 sodium pyruvate, 12 NAC, 10 $MgSO_4$, 0.5 $CaCl_2$, and 25 glucose, around 32°C. Ten minutes after cutting, slices were transferred into oxygenated holding solution (in mM): 94 NaCl, 2.5 KCl, 1.2 NaH_2PO_4, 30 $NaHCO_3$, 20 HEPES, 5 sodium ascorbate, 2 thiourea, 3 sodium pyruvate, 2 $MgSO_4$, 2 $CaCl_2$, 12 NAC, and 25 glucose, under room temperature. After recovery for at least 1 h, the slices were perfused with ACSF (in mM): 124 NaCl, 2.5 KCl, 1.2 NaH_2PO_4, 24 $NaHCO_3$, 5 HEPES, 12.5 glucose, 2 $MgSO_4$ and 2 $CaCl_2$. The recording chamber was on the stage of a BX51WI microscope (Olympus, Shinjuku-ku, Tokyo, Japan) equipped with infrared differential interference contrast optics for visualizing whole cell patch-clamp recordings. Excitatory postsynaptic currents (EPSCs) and action potentials (APs) were recorded from IC with a Digidata 1440A interface, MultiClamp 700B amplifier, and pClamp10 software (Axon Instruments, Sunnyvale, CA, USA). The internal solution of the electrodes (4–8 MΩ tip resistance) contained the following (in mM): 133 K-gluconate, 8 NaCl, 0.6 EGTA, 10 HEPES, 2 Mg-ATP, and 0.3 Na-GTP. The cell type was distinguished under current clamp mode according to the electrophysiological characteristics described by Washburn and Moises in response to intracellular injection of a depolarizing current (100–

300 pA, step 50 pA, duration 1000 ms) [28]. Only the data of excitatory neurons were used for further analyses of sEPSCs. The mEPSCs were recorded in the presence of TTX (1 μM) in the extracellular solution. Series resistance (<20 MΩ) was checked throughout the experiment to ensure high-quality recordings. The membrane potential was held at −70 mV throughout the experiment for EPSC recording. Data were sampled and filtered at 10 kHz.

BzATP (an agonist of P2X7Rs) and BBG (an antagonist of P2X7Rs) were bought from Sigma (St. Louis, MO, USA). A438079, an antagonist of P2X7Rs, was bought from Tocris (Bristol, UK). All drugs were dissolved in ACSF on the day of experiment and added by perfusion.

Histology and Immunofluorescence Study

At the end of the experiment, the site of microinjection was verified following Nissl staining method described previously [23]. The thickness of coronal slices was 30 μm. After staining, the images were analyzed by comparing them to an anatomical atlas. If a site was outside the IC, data of that rat were excluded and not been analyzed. For immunofluorescence, 15-μm frozen sections of slices were simultaneously incubated with synaptophysin (1:100, ab8049, Abcam, Cambridge, UK), P2X7R (1:100, ab93354, Abcam), and IBA-1 (1:1000, 019-19741, Wako, Tokyo, Japan) antibodies for overnight at 4°C and then incubated with secondary antibody with Alexa Fluor 488 and 555 (1:500, Life Technologies Inc., Shanghai, China) for 2 h at room temperature. Negative controls were performed without the primary antibody.

Data Analyses

A fixed length of traces (3 min) of EPSCs was analyzed using MiniAnalysis program 6.0.3 (Synaptosoft, Decatur, GA, USA). Normality was checked for all data before comparisons. Data were analyzed using two-sample *t*-test, Mann–Whitney *U*-test, paired-sample *t*-test, paired-sample Wilcoxon signed-rank test, one-way repeated-measures ANOVA followed by Tukey's *post hoc* test, Dunn's *post hoc* test following Friedman ANOVA with Origin 8 (Origin Lab Inc., Northampton, MA, USA), and Kolmogorov–Smirnov test, as appropriate. All values were shown as mean ± SEM; error bars in the figures stand for SEM. $P < 0.05$ was considered significant.

Results

Enhanced Expression of P2X7 Receptors in IC of NMD Rats

As CVH was induced by NMD at the age 6–7 weeks [22], the expression of P2X7Rs was checked in IC at the same time period after NMD. There was a significant upregulation of P2X7Rs in IC of both hemispheres at protein level as well as at mRNA level when compared with controls (Figure 1A,B, $^{***}P < 0.001$, $^{*}P < 0.05$, n = 4 for each group, two-tailed two-sample *t*-test). However, protein level of P2X1Rs showed a significant upregulation only in left but not right hemisphere of IC in NMD rats compared with controls. In contrast, P2X3Rs showed a significant upregulation only in right but not left side of IC in NMD rats compared with controls (Figure 1C,D, $^{*}P < 0.05$, n = 4 for each group, two-tailed two-sample *t*-test). As P2X7Rs were upregulated in both sides of IC, we therefore focused on the roles of P2X7Rs in the present study.

Hyperexcitation of IC Neurons in NMD Rats

The firing frequency of excitatory neurons of IC slice was next examined for control (CON) and NMD rats. The neurons (n = 17)

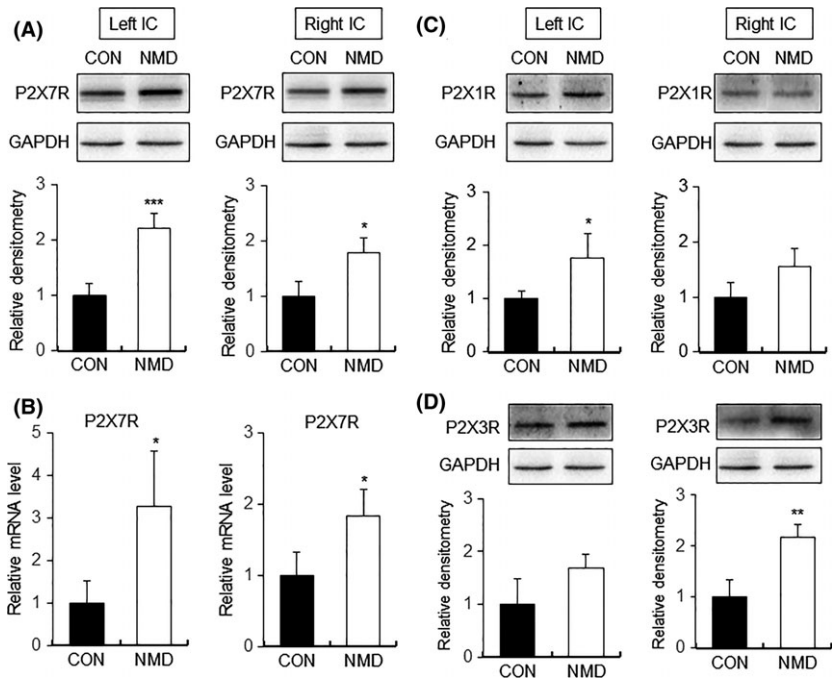

Figure 1 Upregulation of P2X7Rs expression in IC of NMD rats. (**A**) Expression of P2X7Rs at protein level was significantly increased in IC of both hemispheres of NMD rats when compared with age-matched control rats (CON). (**B**) mRNA level of P2X7Rs was markedly enhanced in IC of both hemispheres of NMD group. (**C**) Protein level of P2X1Rs was significantly increased in left but not right hemisphere of IC of NMD rats compared with control rats. (**D**) Protein level of P2X3Rs was obviously increased in right but not left side of IC of NMD rats compared with control rats. n = 4 rats for each group, $^{*}P < 0.05$, $^{**}P < 0.01$, $^{***}P < 0.001$ versus CON.

from NMD rats had a significant higher action potential firing rate than those (n = 15) from control rats at 6–7 weeks of age, under current clamp mode in response to intracellular depolarizing current stimulation at 100 pA (Figure 2A; $*P < 0.05$ vs. CON), Mann–Whitney *U*-test for each current density), indicating the hyperexcitation of IC excitatory neurons of NMD group. However, membrane input resistance, resting membrane potential (RMP), and action potential (AP) threshold were not significantly altered after NMD when compared with controls (Figure 2B–D).

Increase in Glutamatergic Synaptic Activity of IC Neurons in NMD Rats

The spontaneous excitatory postsynaptic currents (sEPSCs) of IC neurons were compared between control and NMD group. The representative traces from two typical neurons of IC slices control and NMD rats illustrated an increase in frequency, without obvious change in amplitude of sEPSCs (Figure 2E). The average results in Figure 2F,G also suggested a significant increase in frequency of sEPSCs in IC of NMD rats (n = 18 for control, n = 9 for NMD, $**P < 0.01$, Mann–Whitney *U*-test).

BzATP Enhanced Glutamatergic Synaptic Activity in IC of Control Groups Through a Presynaptic Mechanism

Activation of P2X7Rs by BzATP, a very potent agonist of P2X7Rs [20], should increase the glutamatergic synaptic activity of IC in control slices. We next showed that BzATP at 30 μM was effective in increasing sEPSCs in seven of seven excitatory neurons tested. The representative current trace (Figure 3A) demonstrated a shortening of interevent intervals with the presence of BzATP in a typical excitatory neuron. It is also shown in the figures of cumulative fraction of peak amplitude and interevent intervals (Figure 3B,C, left). Normalized mean values for amplitude and frequency are shown in Figure 3B,C (right). The results suggested that there was a significant increase in average frequency of sEPSCs (Fig. 3C, right, n = 7, $*P < 0.05$, paired-sample Wilcoxon signed-rank test), without change in its amplitude (Figure 3B, right). In all cells, the sEPSCs were completely blocked by CNQX (10 μM), suggesting that sEPSCs were mediated by non-NMDA receptors (data not shown).

To assess whether BzATP acts on presynaptic or postsynaptic sites in the IC, the amplitude and frequency of mEPSCs were measured in the absence and presence of BzATP in brain slices of control rats. It was proved by Kolmogorov–Smirnov test that BzATP (30 μM) was effective in affecting mEPSCs in six of seven neurons tested. The typical current trace of a single neuron demonstrated an increase in frequency without change in mEPSCs amplitude after the addition of BzATP in IC neurons (Figure 3D). The average results are shown in Figure 3E,F (right, n = 6, $*P < 0.05$, paired-sample Wilcoxon signed-rank test). The present result of mEPSCs suggested the presynaptic activation of P2X7Rs by BzATP in control slices. As it is reported that the activation of P2X7Rs increases the release of presynaptic glutamate [20], we checked this conclusion in this study. No sEPSC was recorded in the presence of CNQX (10 μM) and D-APV (30 μM) with or without BzATP (Figure S1A), which is consistent with the previous report

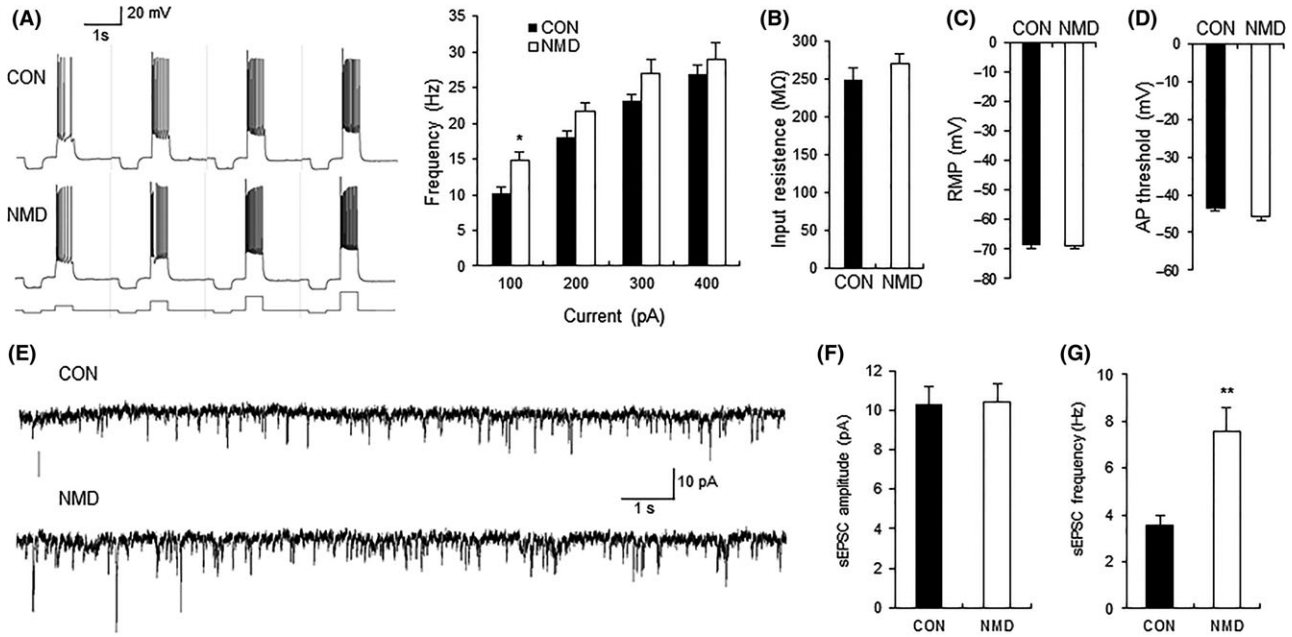

Figure 2 Comparison of membrane properties and sEPSCs of pyramidal neurons between control and NMD group. (**A**) Representative traces of action potential of control (CON) and NMD groups evoked by 100-, 200-, 300-, and 400-pA current stimulation. Bar plot illustrating higher firing frequency of neurons in NMD rats than those in control rats in response to different intensity of injected currents. (**B**) Membrane input resistance, (**C**) resting membrane potential (RMP), and (**D**) action potential (AP) threshold were not altered after NMD. n = 15 cells for control group and n = 17 for NMD group, $*P < 0.05$ versus CON. (**E**) Recordings illustrating sEPSCs of typical neurons in IC of CON (top) and NMD (bottom) rats. (**F**) No change in peak amplitude of sEPSC after NMD. (**G**) Increase in sEPSC frequency in NMD group. n = 18 cells for control group, n = 9 cells for NMD group, $**P < 0.01$ versus CON.

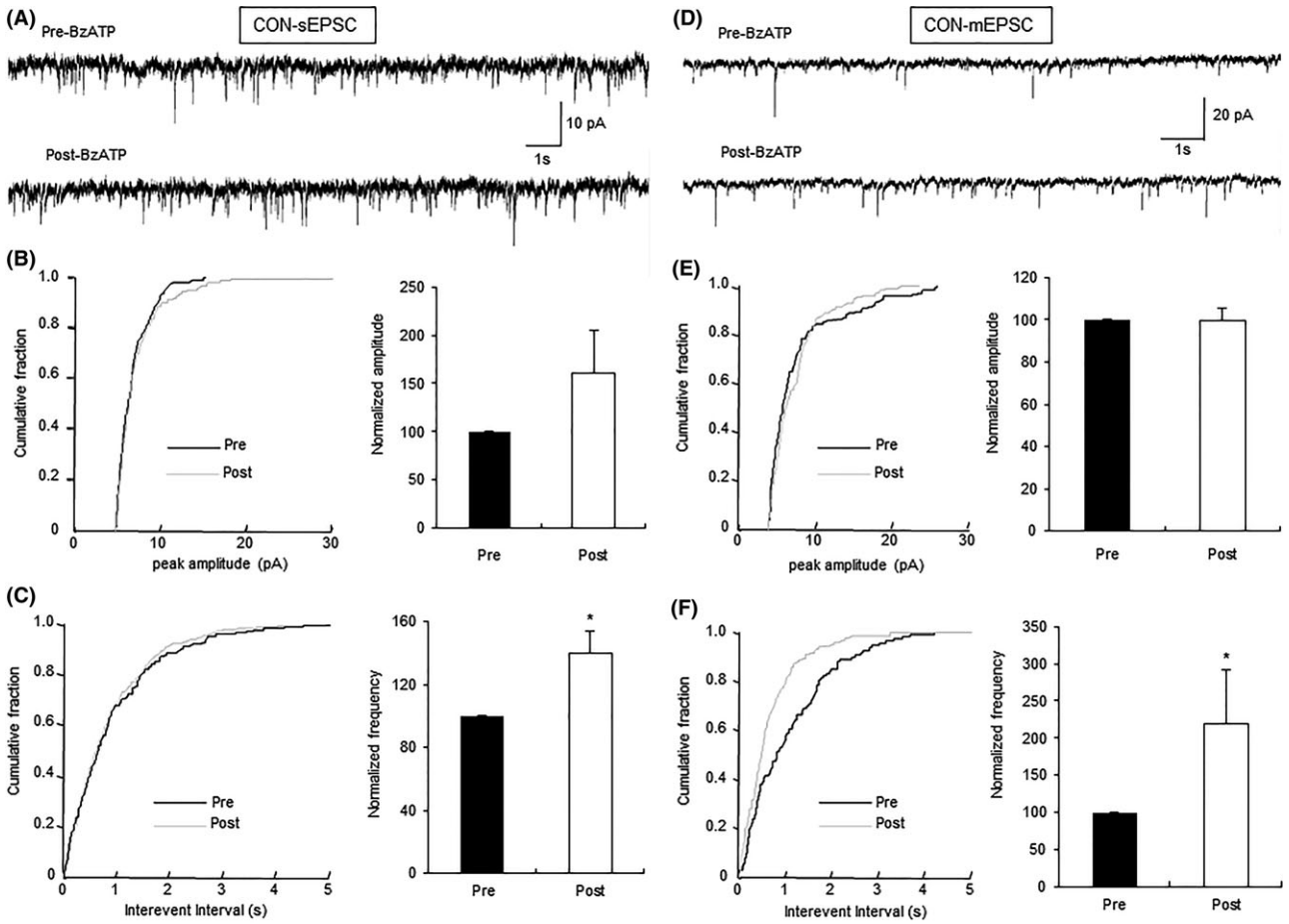

Figure 3 Enhancement of glutamatergic synaptic activity of neurons by BzATP in control rats. (**A**) Representative traces illustrating sEPSCs of an IC neuron of control rats before and after the addition of BzATP (30 μM). (**B**) Cumulative fraction of peak amplitude of sEPSCs in an IC pyramidal neuron under the pre- and postdrug conditions (left); bar plot showing no significant change in sEPSC peak amplitude by BzATP (right). (**C**) Cumulative fraction of interevent intervals of sEPSCs under the pre- and postdrug conditions (left); bar plot showing the significant increase in sEPSC frequency by BzATP (right). n = 7 cells, $^*P < 0.05$ versus pre. (**D**) Representative traces illustrating mEPSCs of an IC neuron before and after the addition of BzATP (30 μM); TTX (1 μM) was used to block action potentials. (**E**) Cumulative fraction of peak amplitude of mEPSCs in one IC pyramidal neuron under the predrug and postdrug conditions (left); bar plot showing no significant change in mEPSC peak amplitude by BzATP (right). (**F**) Cumulative fraction of interevent intervals of mEPSCs under the predrug and postdrug conditions (left); bar plot showing that mEPSC frequency was markedly increased by BzATP treatment (right). Peak amplitude and frequency of BzATP-treated neurons was normalized by that from the same neuron before BzATP treatment. n = 6 cells, $^*P < 0.05$ versus Pre.

[20]. As BzATP has been reported to act also on P2X1 and P2X3 receptors [29], we applied BzATP (30 μM) after the application of A438079, a specific antagonist of P2X7Rs, on control slices. No significant excitatory effect on sEPSC of IC neurons was observed for BzATP with the presence of A438079 (Figure S1B–D).

Expression of P2X7Rs in IC

The distribution of P2X7Rs in IC was determined by immunofluorescence study. The anatomy on the brain marked by nucleus marker DAPI and the brain atlas pointed the site of IC (Figure 4A,B). P2X7Rs were also colocalized with NeuN, a marker of neurons (Figure 4C). As shown in Figure 4D, many P2X7Rs were colocalized with synaptophysin, a marker of presynaptic sites [30]. The result is consistent with the presynaptic mechanism of P2X7Rs as suggested by our electrophysiological studies. Only very few P2X7Rs colocalized with IBA-1 (a marker of microglia cells) and GFAP (a marker of astrocyte cells), as shown in Figure 4E,F.

BBG Reduced Glutamatergic Synaptic Activity of IC Neurons in NMD Group Through a Presynaptic Mechanism

Brilliant blue G (BBG), an antagonist of P2X7Rs, was used in this study to affect sEPSCs of excitatory neurons of IC slices in NMD rats. The typical current traces (Figure 5A), the cumulative fraction of peak amplitude and interevent intervals for a representative neuron (Figure 5B,C, left), and normalized mean values for amplitude and frequency (Figure 5B,C, right, n = 6, $^*P < 0.05$, paired-sample Wilcoxon signed-rank test) all suggested that

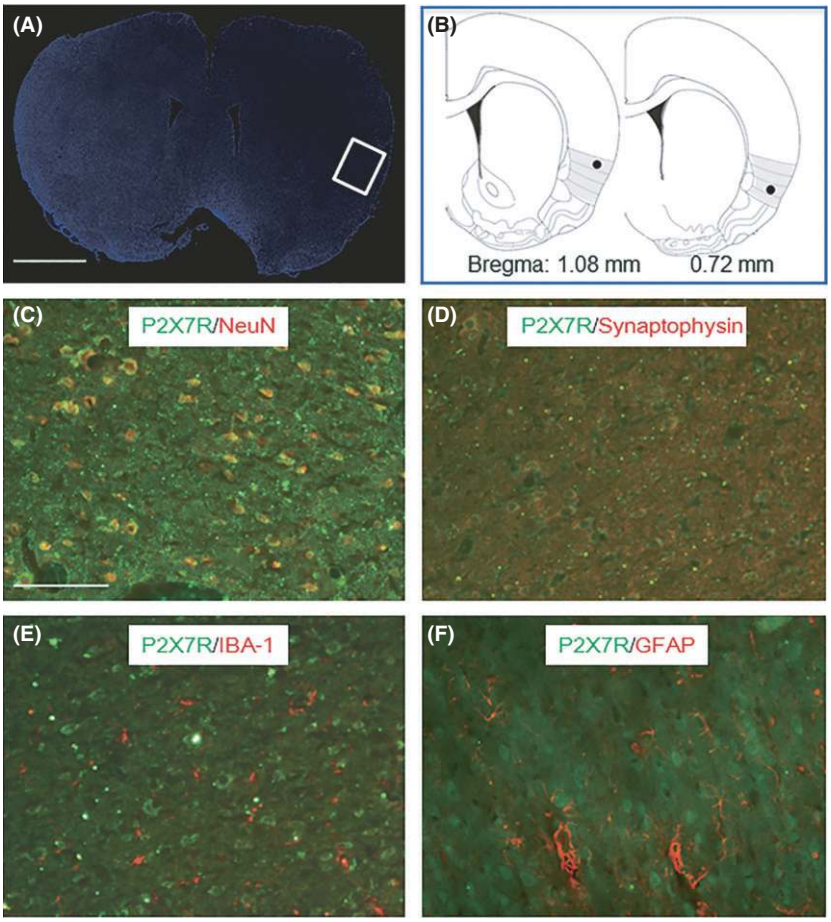

Figure 4 Colocalization of P2X7Rs and IC cells. (**A**) The anatomy on the brain dyed by nucleus marker DAPI, and IC part is pointed by white box. (**B**) Brain atlas shows the site of IC. Black spots represent the microinjection position. (**C**, **D**, **E**, **F**) P2X7Rs are marked by green dots. (**C**) Neurons were marked by NeuN in red dots. (**D**) Presynaptic sites were marked by synaptophysin in red dots. (**E**) Microglia cells were marked by IBA-1 in red dots. (**F**) Astrocyte cells were marked by GFAP in red dots. Scale bar in Figure **A** and **C** equals 2 mm and 100 μm, respectively.

blockade of P2X7Rs decreased the frequency of sEPSCs of IC neurons in NMD rats, without change in amplitude (Figure 5B, right). To further assess whether BBG acts on presynaptic or postsynaptic sites in the IC, the frequency and amplitude of mEPSCs were measured in the absence and presence of BBG in IC slices of NMD rats. The typical current traces (Figure 5D), the cumulative fraction of peak amplitude and interevent intervals for a representative neuron (Figure 5E,F, left), and normalized mean values for amplitude and frequency (Figure 5E,F, right, n = 6, $^{*}P < 0.05$, paired-sample Wilcoxon signed-rank test) all suggested that the blocking site of P2X7Rs by BBG is most likely presynaptic, which is consistent with the finding that the site of activation of P2X7Rs in IC slices was presynaptic in control rats.

BzATP Induced Visceral Hypersensitivity in Control Rats and BBG or A438079 Reversed Visceral Hypersensitivity in NMD Rats

We then microinjected BzATP into right hemisphere of IC to examine the effect of BzATP in control rat. Microinjection of BzATP led to a large decrease in the CRD threshold in control rats. The microinjection sites are shown in Figures 6A and 4B. The significant hyperalgesia effect was observed at 30 μM BzATP (Figure 6B, n = 6 for each group, $^{*}P < 0.05$ vs. NS, Tukey's *post hoc* test following one-way repeated-measures ANOVA) and lasted for 15 min (Figure 6C, n = 7 for each group, $^{***}P < 0.001$ vs. NS, Dunn's *post hoc* test following Friedman ANOVA), which was consistent with previous reports [31]. We next examined the effect of blockade of P2X7Rs on visceral hypersensitivity of NMD rats. Injection of BBG (0.1 or 1 μM) significantly increased CRD threshold in NMD rats with a bigger effect at 1 μM when tested 5 min after BBG injection (Figure 6D, n = 6 for each group, $^{*}P < 0.05$ vs. NS, $^{**}P < 0.01$ vs. NS, Tukey's *post hoc* test following one-way repeated-measures ANOVA). The analgesia effect of BBG at dose of 1 μM disappeared when tested 15 min postinjection (Figure 6E, n = 6 for each group, $^{***}P < 0.001$, $^{**}P < 0.01$ vs. NS, Tukey's *post hoc* test following one-way repeated-measures ANOVA). The effect of A438079, another highly selective antagonist of P2X7Rs [32], on CRD threshold in NMD rats was also determined. A438079 (500 or 1 mM) significantly increased CRD threshold (Figure 6G, n = 5 for each group, $^{*}P < 0.05$ for 500 nM, $^{**}P < 0.01$ for 1 mM, paired-sample *t*-test) when tested 5 min postinjection. The analgesia effect of A438079 (1 mM) existed at 5 min postinjection (Figure 6H, n = 5 for each group, $^{**}P < 0.01$ vs. vehicle, Tukey's *post hoc* test following one-way repeated-measures ANOVA). A438079 (1 mM) did not alter CRD threshold in age-matched healthy control rats (Figure 6F, n = 6 for each group).

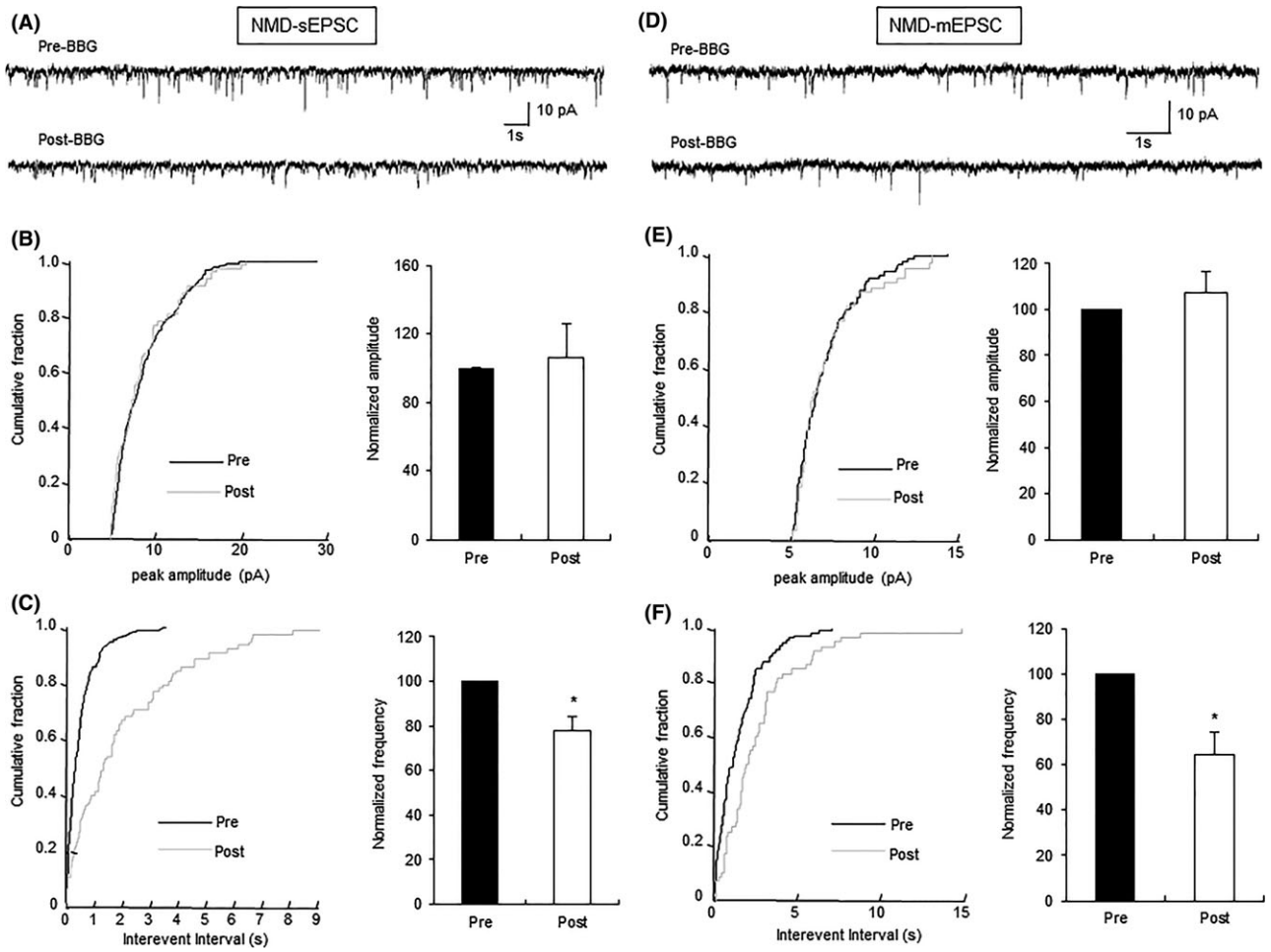

Figure 5 Decrease in glutamatergic synaptic activity of IC neurons by BBG in NMD rats. (**A**) Representative traces illustrating sEPSCs of an IC neuron before and after the addition of BBG (1 μM). (**B**) Cumulative fraction of peak amplitude of sEPSCs in an IC pyramidal neuron under the pre- and postdrug conditions (left); bar plot showing no significant change in sEPSC peak amplitude by BBG (right). (**C**) Cumulative fraction of interevent intervals of sEPSCs under the pre- and postdrug conditions (left); bar plot showing the significant decrease in sEPSC frequency by BBG (right). n = 6 cells, $^*P < 0.05$ versus pre. (**D**) Representative traces illustrating mEPSCs of an IC neuron before and after the addition of BBG (1 μM); TTX (1 μM) was used to block action potentials. (**E**) Cumulative fraction of peak amplitude of mEPSCs in one IC pyramidal neuron under the pre- and postdrug conditions (left); bar plot showing no significant change in mEPSC peak amplitude by BBG (right). (**F**) Cumulative fraction of interevent intervals of mEPSCs under the pre- and postdrug conditions (left); bar plot showing that mEPSC frequency was remarkably decreased by BBG treatment (right). Peak amplitude and frequency of BBG-treated neurons were normalized by those from the same neuron before BBG treatment. n = 6 cells, $^*P < 0.05$ versus pre.

Discussion

IC is involved in peripheral nerve ligation-induced neuropathic pain [33], CFA-induced hyperalgesia [34], phantom limb pain of human [6], but not in acute pain [35]. In the present study, although the expression of P2X7Rs upregulated in both hemispheres of IC, microinjection of P2X7R agonist into right IC was efficient to induce visceral hypersensitivity in control rats and microinjection of P2X7R antagonist reversed CVH in NMD rats. These findings suggested that P2X7Rs in right IC plays an important role in the development of visceral pain induced by NMD, as being consistent with the more strong structural connections to autonomic control areas of right IC [24]. P2X7R was also reported to play roles in the development of inflammatory pain [31], neuropathic hyperalgesia [36], and IBS [37]. In addition to roles of P2X7R in IC, the increased expression of P2X7Rs in dorsal root ganglion enhanced visceral pain, just like the increased expression of P2X4 and P2X6 receptors [38]. However, this study does not exclude the roles of the other subtypes of purinergic receptors in the development and maintenance of visceral hypersensitivity of NMD rats.

Under normal conditions, the expression of P2X7Rs in neurons, astrocytes, glial cells, and nonactivated microglia is low [31]. However, in the present study the expression of P2X7Rs was significantly increased in IC of NMD rats although very few P2X7Rs were expressed on microglial cells and astrocytes in the IC. In the present study, there is an increase in frequency of mEPSCs by BzATP, without significant alteration in amplitude of mEPSCs.

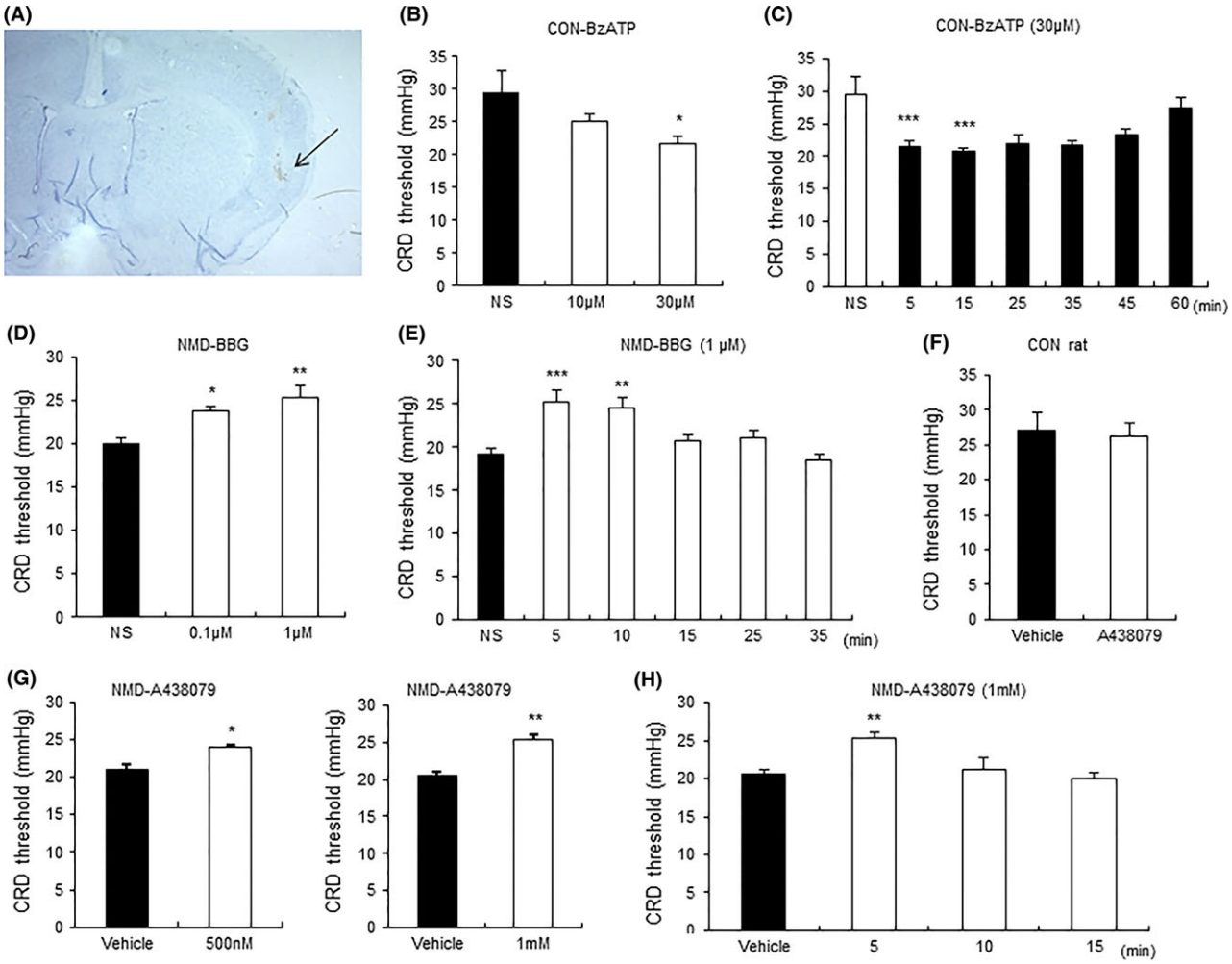

Figure 6 Modulation of CRD threshold by microinjection of agonist and antagonists of P2X7R into IC. (**A**) A representative picture of actual track of microinjection in the IC of right hemisphere as pointed out by the black arrow. (**B**) Bar plot illustrating a dose effect of BzATP. There is a significant decrease in CRD threshold in control rats by 30 μM BzATP when tested 5 min after microinjection. n = 6 rats for each group, $^{*}P < 0.05$ versus normal saline (NS). (**C**) Bar plot illustrating the time course of the effect of BzATP (30 μM). BzATP significantly decreased CRD threshold when tested at 5 and 15 min postinjection. n = 7 rats for each group, $^{***}P < 0.001$ versus NS for each time point. (**D**) Bar plot showing the dose effect of BBG. There is a significant increase in CRD threshold in NMD rats by BBG (0.1 and 1 μM) when tested 5 min after microinjection, with bigger effect at 1 μM. n = 6 rats for each group, $^{*}P < 0.05$, $^{**}P < 0.01$ versus NS. (**E**) Bar plot showing the time course of the effect of BBG (1 μM). There is a significant increase in CRD threshold in NMD rats when tested at 5 and 10 min after microinjection. n = 6 rats for each group, $^{**}P < 0.01$, $^{***}P < 0.001$ versus NS. (**F**) Bar plots showing no change in CRD threshold of control rats by A438079 (1 mM). n = 6 rats for each group. (**G**) Bar plots showing an increase in CRD threshold in NMD rats by both 500 nM and 1 mM A438079 when tested 5 min after microinjection. n = 5 rats for each group, $^{*}P < 0.05$, $^{**}P < 0.01$ versus vehicle. (**H**) Bar plot showing the time course of the effect of A438079 (1 mM). There is a significant increase in CRD threshold in NMD rats when tested at 5 min after microinjection. n = 5 rats for each group, $^{**}P < 0.01$ versus vehicle.

The result suggested the presynaptic action of P2X7Rs. Furthermore, NMD only increased the frequency of action potentials without changing the resting membrane potential, action potential threshold, and input resistance of IC neurons. This result could further support the presynaptic mechanism. In addition, P2X7Rs colocalized with synaptophysin and NeuN in IC. As P2X7R is a ligand-gated nonselective cation channel and no EPSC was evoked by BzATP in the presence of CNQX and D-APV, it is therefore reasonable to hypothesize that the P2X7R was not functionally expressed in the cell body but was functionally expressed in presynaptic part, which is consistent with the electrophysiological data.

It is reported that peripheral nerve ligation of mice enhanced AMPA receptor-mediated excitatory synaptic transmission in the IC [39]. This effect relies on the GluR1 subunit of AMPA receptor on synapses [40], and probably by inhibiting endocytosis at the cell membrane or increasing exocytosis of GluR1 at external sites of synapses to improve the AMPA receptor-mediated synaptic transmission [41]. However, this seems not to be the case in IC of NMD rats as there was only an increase in frequency without

change in amplitude of sEPSC in NMD group when compared with control group.

Besides P2X7R, several other modulators might contribute to the overexcitation of IC in NMD rats. These modulators include PKMζ, GluR2 [5], phosphorylated ERK-1/2, pCREB, c-Fos, GABA, dopamine [34], P2X7R-mediated d-serine release [42], opioids [43]. P2X7Rs are reported to play an upstream transductional role in the development of neuropathic and inflammatory pain via the regulation of IL-1β production [31]. The mRNA level of IL-1β was significantly increased in IC of both hemispheres in NMD rats (data not shown), suggesting that IL-1β may also contribute to visceral hypersensitivity of NMD rats. There is also a growing body of evidence showed that P2X7Rs can attribute to inflammation in lung, heart, and islet transplantation and that oATP (P2X7R inhibitor) could reverse the effect [44–46]. In addition, stress mediators and the gut microbiota can interact through complementary or opposing factors to influence visceral sensitivity [47]. Investigation of roles of inflammation and immune system is definitely needed.

In addition to IC, there are several other parts of central nervous system taking part in modulation of visceral pain. It is proved that the overexcitation of basolateral amygdala contributed to the visceral hypersensitivity of NMD rats [23]. The amygdala, particularly the basal complex, and the nucleus accumbens are important targets of IC efferent fibers [43]. The overexcitation of amygdala may be resulted from the overexcitation of IC in NMD rats. IC also modulates pain through affecting middle cingulate cortex, periaqueductal gray, locus coeruleus, the nucleus accumbens, or raphe nucleus [43]. The spinal cord, the first relay center for nociceptive processing, is worthy of exploring pain mechanism and effects of antinociceptive drugs [48]. The detailed neural circuitry among these areas definitely needs to be further investigated.

Conclusion

In conclusion, the present study provided evidence that upregulation of P2X7Rs in IC increased glutamate neurotransmission and sensitized the IC neurons through a presynaptic mechanism, which resulted in the visceral hypersensitivity of NMD rats. Modulation of IC in right hemisphere by drugs could modulate pain processing.

Acknowledgments

This work was supported by grants from National Natural Science Foundation of China (31300909 to YX, 81230024 and 81471137 to GYX) and from the Priority Academic Program Development of Jiangsu Higher Education Institutions of China. The funders had no role in the study design, data collection and analysis, decision to publish, or preparation of the manuscript.

Conflict of Interest

The authors declare no conflict of interest.

References

1. Gauriau C, Bernard JF. Posterior triangular thalamic neurons convey nociceptive messages to the secondary somatosensory and insular cortices in the rat. *J Neurosci* 2004;**24**:752–761.
2. Benison AM, Chumachenko S, Harrison JA, et al. Caudal granular insular cortex is sufficient and necessary for the long-term maintenance of allodynic behavior in the rat attributable to mononeuropathy. *J Neurosci* 2011;**31**:6317–6328.
3. Baier B, Eulenburg PZ, Geber C, et al. Insula and sensory insular cortex and somatosensory control in patients with insular stroke. *Eur J Pain* 2014;**18**:1385–1393.
4. Henderson LA, Gandevia SC, Macefield VG. Somatotopic organization of the processing of muscle and cutaneous pain in the left and right insula cortex: A single-trial fMRI study. *Pain* 2007;**128**:20–30.
5. Han J, Kwon M, Cha M, et al. Plasticity-related PKMζ Signaling in the insular cortex is involved in the modulation of neuropathic pain after nerve injury. *Neural Plast* 2015;**2015**:601767.
6. Liu MG, Zhuo M. Loss of long-term depression in the insular cortex after tail amputation in adult mice. *Mol Pain* 2014;**10**:1.
7. Hanamori T, Kunitake T, Kato K, et al. Responses of neurons in the insular cortex to gustatory, visceral, and nociceptive stimuli in rats. *J Neurophysiol* 1998;**79**:2535–2545.
8. Craig AD. How do you feel? Interoception: The sense of the physiological condition of the body. *Nat Rev Neurosci* 2002;**3**:655–666.
9. Lu C, Yang T, Zhao H, et al. Insular cortex is critical for the perception, modulation, and chronification of pain. *Neurosci Bull* 2016;**32**:191–201.
10. Morgan V, Pickens D, Gautam S, et al. Amitriptyline reduces rectal pain related activation of the anterior cingulate cortex in patients with irritable bowel syndrome. *Gut* 2005;**54**:601–607.
11. Nedergaard MLCM. Physiological and pathological functions of P2X7 receptor in the spinal cord. *Purinergic Signalling* 2009;**5**:223–232.
12. Guthrie PB, Knappenberger J, Segal M, et al. ATP released from astrocytes mediates glial calcium waves. *J Neurosci* 1999;**19**:520–528.
13. Kennedy C, Saville VL, Burnstock G. The contributions of noradrenaline and ATP to the responses of the rabbit central ear artery to sympathetic nerve stimulation depend on the parameters of stimulation. *Eur J Pharmacol* 1986;**122**:291–300.
14. Jo YH, Schlichter R. Synaptic corelease of ATP and GABA in cultured spinal neurons. *Nat Neurosci* 1999;**2**:241–245.
15. León D, Sánchez-Nogueiro J, Marín-García P, et al. Glutamate release and synapsin-I phosphorylation induced by P2X 7 receptors activation in cerebellar granule neurons. *Neurochem Int* 2008;**52**:1148–1159.
16. Yu Y, Ugawa S, Ueda T, et al. Cellular localization of P2X7 receptor mRNA in the rat brain. *Brain Res* 2008;**1194**:45–55.
17. Li N, Zhang P, Qiao M, et al. The effects of early life lead exposure on the expression of P2X7 receptor and synaptophysin in the hippocampus of mouse pups. *J Trace Elem Med Biol* 2015;**30**:124–128.
18. North RA. Molecular physiology of P2X receptors. *Physiol Rev* 2002;**82**:1013–1067.
19. Marcoli M, Cervetto C, Paluzzi P, et al. P2X7 pre-synaptic receptors in adult rat cerebrocortical nerve terminals: A role in ATP-induced glutamate release. *J Neurochem* 2008;**105**:2330–2342.
20. Deuchars SA, Atkinson L, Brooke RE, et al. Neuronal P2X7 receptors are targeted to presynaptic terminals in the central and peripheral nervous systems. *J Neurosci* 2001;**21**:7143–7152.
21. Armstrong JNMB. P2X7-receptor activation depresses synaptic transmission at hippocampal mossy fiber-CA3 synapses. *Soc Neurosci Abstr* 2000;**26**:884.
22. Hu S, Xiao Y, Zhu L, et al. Neonatal maternal deprivation sensitizes voltage-gated sodium channel currents in colon-specific dorsal root ganglion neurons in rats. *Am J Physiol Gastrointest Liver Physiol* 2013;**304**:G311–G321.
23. Xiao Y, Chen X, Zhang PA, et al. TRPV1-mediated presynaptic transmission in basolateral amygdala contributes to visceral hypersensitivity in adult rats with neonatal maternal deprivation. *Sci Rep* 2016;**6**:29026.
24. Macey PM, Wu P, Kumar R, et al. Differential responses of the insular cortex gyri to autonomic challenges. *Auton Neurosci* 2012;**168**:72–81.
25. Browne LE, North RA. P2X receptor intermediate activation states have altered nucleotide selectivity. *J Neurosci* 2013;**33**:14801–14808.
26. Guo J, Fu X, Cui X, et al. Contributions of purinergic P2X3 receptors within the midbrain periaqueductal gray to diabetes-induced neuropathic pain. *J Physiol Sci* 2015;**65**:99–104.
27. Ting JT, Daigle TL, Chen Q, et al. Acute brain slice methods for adult and aging animals: application of targeted patch clamp analysis and optogenetics. *Methods Mol Biol* 2014;**1183**:221–242.
28. Washburn MS, Moises HC. Electrophysiological and morphological properties of rat basolateral amygdaloid neurons in vitro. *J Neurosci* 1992;**12**:4066–4079.
29. Bianchi BR, Lynch KJ, Touma E, et al. Pharmacological characterization of recombinant human and rat P2X receptor subtypes. *Eur J Pharmacol* 1999;**376**:127–138.
30. Okabe S, Miwa A, Okado H. Spine formation and correlated assembly of presynaptic and postsynaptic molecules. *J Neurosci* 2001;**21**:6105–6114.

31. Kuan YH, Shyu BC. Nociceptive transmission and modulation via P2X receptors in central pain syndrome. *Mol Brain* 2016;**9**:58.
32. Leichsenring A, Riedel T, Qin Y, et al. Anoxic depolarization of hippocampal astrocytes: Possible modulation by P2X7 receptors. *Neurochem Int* 2013;**62**: 15–22.
33. Moriarty O, McGuire BE, Finn DP. The effect of pain on cognitive function: A review of clinical and preclinical research. *Prog Neurobiol* 2011;**93**:385–404.
34. Peltz E, Seifert F, DeCol R, et al. Functional connectivity of the human insular cortex during noxious and innocuous thermal stimulation. *NeuroImage* 2011;**54**:1324–1335.
35. Coffeen U, Ortega-Legaspi JM, Lopez-Munoz FJ, et al. Insular cortex lesion diminishes neuropathic and inflammatory pain-like behaviours. *Eur J Pain* 2011;**15**:132–138.
36. Kobayashi K, Takahashi E, Miyagawa Y, et al. Induction of the P2X7 receptor in spinal microglia in a neuropathic pain model. *Neurosci Lett* 2011;**504**:57–61.
37. Keating C, Pelegrin P, Martinez CM, et al. P2X7 receptor-dependent intestinal afferent hypersensitivity in a mouse model of postinfectious irritable bowel syndrome. *J Immunol* 2011;**187**:1467–1474.
38. Chen L, Liu YW, Yue K, et al. Differential expression of ATP-gated P2X receptors in DRG between chronic neuropathic pain and visceralgia rat models. *Purinergic Signalling* 2016;**12**:79–87.
39. Qiu S, Zhang M, Liu Y, et al. GluA1 phosphorylation contributes to postsynaptic amplification of neuropathic pain in the insular cortex. *J Neurosci* 2014;**34**:13505–13515.
40. Kam AY, Liao D, Loh HH, et al. Morphine induces AMPA receptor internalization in primary hippocampal neurons via calcineurin-dependent dephosphorylation of GluR1 subunits. *J Neurosci* 2010;**30**:15304–15316.
41. Oh MC, Derkach VA, Guire ES, et al. Extrasynaptic membrane trafficking regulated by GluR1 serine 845 phosphorylation primes AMPA receptors for long-term potentiation. *J Biol Chem* 2006;**281**:752–758.
42. Pan HC, Chou YC, Sun SH. P2X7 R-mediated Ca(2+) -independent d-serine release via pannexin-1 of the P2X7 R-pannexin-1 complex in astrocytes. *Glia* 2015;**63**:877–893.
43. Jasmin L, Burkey AR, Granato A, et al. Rostral agranular insular cortex and pain areas of the central nervous system: A tract-tracing study in the rat. *J Comp Neurol* 2004;**468**:425–440.
44. Andrea Vergani CF, D'Addio F, Tezza S, et al. Effect of the purinergic inhibitor oxidized ATP in a model of islet allograft rejection. *Diabetes* 2013;**62**:1665–1675.
45. Andrea Vergani ST, D'Addio F, Fotino C, et al. Long-term heart transplant survival by targeting the ionotropic purinergic receptor P2X7. *Circulation* 2013;**127**:463–475.
46. Liu K, Vergani A, Zhao P, et al. Inhibition of the purinergic pathway prolongs mouse lung allograft survival. *Am J Respir Cell Mol Biol* 2014;**51**:300–310.
47. Moloney RD, Johnson AC, O'Mahony SM, et al. Stress and the microbiota-gut-brain axis in visceral pain: Relevance to irritable bowel syndrome. *CNS Neurosci Ther* 2016;**22**:102–117.
48. Rivera-Arconada I, Roza C, Lopez-Garcia JA. Spinal reflexes and windup in vitro: Effects of analgesics and anesthetics. *CNS Neurosci Ther* 2016;**22**:127–134.

Supporting Information

The following supplementary material is available for this article:

Figure S1. BzATP increased sEPSC of IC through release of glutamate in control group.

